



Dynamic Characteristics of the Doubly-Fed Induction Generator Based Wind Turbine under Grid Fault Conditions

T. T. Phan, V. L. Nguyen, P. T. Huynh and H. T. Tran

Abstract— The Doubly-fed induction generator (DFIG) wind turbine (WT) is an integrated part of distributed generation system. The use of DFIG in wind farms is growing rapidly because of its advantages in decoupled active and reactive power control. However, one of the main disadvantages of DFIG is that it is very sensitive to grid faults. To analysis dynamic behaviors of DFIG during grid faults, a model including wind wheel, wind speed, drive train, generator, and converters has been proposed. This paper examines the use of distribution static compensator (D-STATCOM) as a dynamic voltage restorer at the point of common coupling (PCC) to improve the grid fault ride-through (FRT) capability and thereby protecting system stability during disturbances. The simulation results illustrate the comparative dynamic characteristics of the DFIG based wind turbine when a sudden short circuit at PCC is introduced. Besides, the paper also shows detailed comparisons of the transient behaviors between DFIG and conventional induction generator wind turbine under grid fault conditions.

Keywords— Doubly-fed induction generator, active and reactive power control, distribution static compensator, grid fault ride-through capability.

1. INTRODUCTION

Since wind energy is expected to play an important role in the future energy industry, wind power generation technology has received world-wide attention. Wind power generation based on the doubly-fed induction generator (DFIG) has gained increasing popularity due to several advantages, including smaller converter ratings around 30% of the generator rating, variable speed and decoupled active and reactive power control capabilities, lower converter cost, and power losses compared with the fixed speed induction generators or synchronous generators with full-sized converters [1]. However, DFIG easily suffers from the effect of power system disturbances [2]. As the power penetration from the DFIG-based WTs into the grid has increased steadily in recent years, the grid codes require that the wind power generators should not be tripped from the grid but stay connected during the fault conditions [3], which mean that the WTs need to have the capability of fault ride through. Moreover, in many countries, the modern grid codes stipulated specifically the voltage sag and over-current in the rotor side converter (RSC) profile because RSC is a vulnerable part of the DFIG power converter, which has a restricted over-current limits [4]. This is also referred as FRT requirements. At present, low voltage ride-through (LVRT) of DFIG, which is one of the main content of FRT, is studied widely and many

improvement approaches are provided by scholars. However, there are seldom researchers to work on over-current of DFIG for improving FRT, which caused by power system disturbances. When a fault occurs in the power system, over-current in the RSC of WTs will threaten the generator's security, which even leads to a serious WT generators tripping accident. So it is extremely important to maintain current in the rotor side converter in the DFIG during the period of disturbances.

X. Kong [5] and J. Ouyang [6] have discussed the dynamic behavior of the fault current of the DFIG under non-severe fault conditions. However, the research results are based on symmetric fault conditions, and there are no analytical expressions of the fault current under asymmetrical fault conditions. One of the most severe problems of the DFIG under asymmetrical faults is the oscillation of stator output power and electromagnetic torque, which are harmful to the stability of the connected power grid and the mechanical system of the WT [7]. An analytical transient model of a doubly fed induction machine and its experimental validation is described in [8]. Detailed simulation transient analysis of a 2 MW wind power DFIG including a model of control and crowbar protection under grid disturbances is presented in [9]. According to [10] and [11], the three phase analytical model of a DFIG for stability studies and its transient behaviors were presented and benchmarked with the advanced model. Nevertheless, in most of the above mentioned papers, the authors only focused on establishing an analytical model of DFIG and investigating its dynamic performances during the period of disturbances, and they neglected technical solutions which can help overcoming or alleviating impacts caused by grid disturbances.

The paper also proposes using D-STATCOM as one of the most interesting solutions to improve FRT capability of wind farms based on DFIG directly connected to the

T. T. Phan (corresponding author), P. T. Huynh and H. T. Tran is with Faculty of Electrical, Electronics and Telecommunication Engineering, Can Tho University of Technology, 256 Nguyen Van Cu, Dist. Ninh Kieu, Can Tho City, Vietnam. Email: {pptuan, hpriren, thtam}@ctu.edu.vn.

V. L. Nguyen is with Faculty of Electrical Electronics Engineering, HCMUT, 268 Ly Thuong Kiet St., Dist. 10, Ho Chi Minh City, Vietnam. E-mail: nvliem@hcmut.edu.vn.

grid. For this purpose, the D-STATCOM is controlled to regulate the wind farm terminal bus voltage through the reactive power exchange with the network [12], [13]. When system voltage drops due to grid faults, the D-STATCOM injects immediately reactive power on the connection point in an attempt to limit the voltage dip. Control techniques commonly used are based on ac-positive sequence voltage and current measured at the connection point. Therefore, depending on the voltage dip, the D-STATCOM injects the same amount of reactive power in all of the three phases. This control technique is suitable when the D-STATCOM is operated under symmetrical conditions, such as following three phase short circuits when all the three grid voltages have the same drop amplitude and the system remains symmetrical. Although symmetrical faults are the most severe ones, its occurrence is extremely rare. In contrast, asymmetrical faults, which occur when one or two phases are shorted to ground or to each other, happen most often, leading to the appearance of the negative sequence component in the grid voltages. Thus, the performance of the D-STATCOM when facing asymmetrical faults and the impacts on dynamic responses of DFIG in these situations needs to be evaluated.

The paper has been organized in some sections as follows. In Section 2, the modelization of the system including DFIG is discussed. The structure and operation of D-STATCOM are presented in Section 3. The model validation is presented in Section 4, showing the results of system transient responses from simulation and comparative behaviors between DFIG and conventional induction generator WT. Finally, the conclusions are summarized in Section 5.

2. MODELING OF DFIG WIND TURBINE

2.1. Wind wheel modeling

Wind turbine electrical generation system (WTGS) power comes from the kinetic energy of the wind, thus it can be expressed as the kinetic power available in the stream of air multiplied by a C_p factor called power coefficient or Betz's factor. The mechanical power extracted by the WT has the following expression:

$$P_{mech} = C_p P_{wind} = C_p \frac{1}{2} \rho A v^3 \quad (1)$$

where C_p is the power coefficient, ρ is the air density and A is the area swept by the rotor. In Fig. 1, an example of a $C_p(\lambda, \beta)$ curve can be seen with the power coefficient, C_p , as a function of the tip speed ratio, λ .

There have been different approaches to model the power coefficient ranging from considering it to be constant for steady state and small signal response simulations to using lookup tables with measured data. Another common approach is to use an analytic expression of the form:

$$C_p(\lambda, \beta) = c_1 \left(c_2 \frac{1}{\lambda_i} - c_3 \beta - c_4 \beta^{c_5} - c_6 \right) e^{-c_7 \frac{1}{\lambda_i}} \quad (2)$$

where λ is the so called tip-speed ratio and it is defined

as:

$$\lambda = \frac{\Omega_r R}{v} \quad (3)$$

where Ω_r is the turbine speed, R is the turbine radius and λ_i is defined as:

$$\frac{1}{\lambda_i} = \frac{1}{\lambda + c_8 \beta} - \frac{c_9}{1 + \beta^3} \quad (4)$$

where $[c_1, \dots, c_9]$ are characteristic constants for each WT and β is the blade pitch angle.

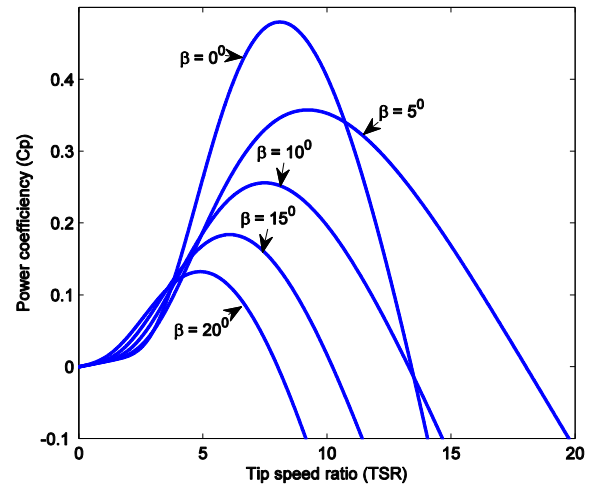


Fig.1. Power coefficient, C_p , as a function of TSR, λ .

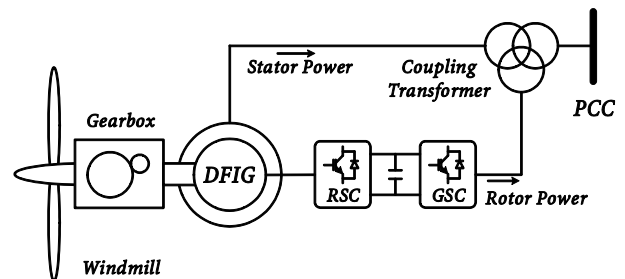


Fig.2. Configuration of a DFIG wind turbine.

Thus by knowing the wind speed, the angular speed of the WT and the blade pitch angle, the mechanical torque on the turbine shaft can be easily computed.

2.2. Wind speed modeling

One possible approach to generate the wind speed signal on simulations may be to use logs of real measurements of the speed on the real location of the WTGS. This approach has some evident limitations because it requires a measurement to be done in each place to be simulated. Another choice in [14] is to use a mathematical model which takes some landscape parameters to generate a wind speed sequence for any location. This wind speed expression has the form:

$$v(t) = v_{avg} + v_r(t) + v_g(t) + v_t(t) \quad (5)$$

where v_{avg} an average wind speed, $v_r(t)$ is a common ramp component, $v_g(t)$ is a gust component and $v_t(t)$ is

a turbulence component.

Wind speed ramp component can be written as a function of time t :

$$v_r(t) = \begin{cases} 0, & t \leq T_{r1} \\ \widehat{A}_r \left(\frac{t - T_{r1}}{T_{r2} - T_{r1}} \right), & T_{r1} < t \leq T_{r2} \\ \widehat{A}_r, & t > T_{r2} \end{cases} \quad (6)$$

where T_{r1} and T_{r2} are the times at which the ramp starts and ends respectively and \widehat{A}_r is the ramp maximum.

The gust component may be useful to simulate an abnormal temporary increase of the speed of the wind and its expression is:

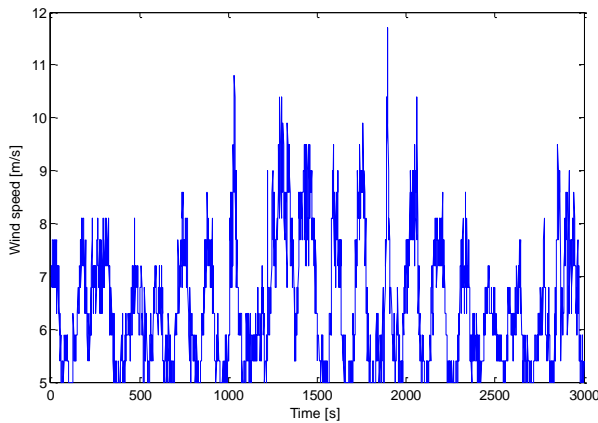


Fig.3. Wind speed used for simulation.

$$v_g(t) = \begin{cases} 0, & t \leq T_{g1} \\ \frac{\widehat{A}_g}{2} \left(1 - \cos \left[2\pi \frac{t - T_{g1}}{T_{g2} - T_{g1}} \right] \right), & T_{g1} < t \leq T_{g2} \\ 0, & t > T_{g2} \end{cases} \quad (7)$$

where T_{g1} and T_{g2} are the times at which the gust starts and ends respectively and \widehat{A}_g is the peak of the gust.

The turbulence of a wind speed sequence can be written as a sum of sinusoidal functions:

$$v_t(t) = \sqrt{2} \sum_{i=1}^N \sqrt{\Delta\omega s(\omega_i)} \cos(\omega_i' t + \varphi) \quad (8)$$

where $\omega_i = \left(1 - \frac{1}{2}\right) \Delta\omega$ (rad/s) and the phase angle φ is uniformly distributed between 0 and 2π .

The function $s(\omega)$ is the spectral density function defined by the following equation:

$$s(\omega) = u^2 \frac{105 \frac{z}{v_{avg}}}{\left(1 + 33 \frac{z\omega_i}{2\pi v_{avg}}\right)^{\frac{5}{3}}} \quad (9)$$

$$u = \frac{0.4 v_{avg}}{\ln \frac{z}{z_0}} \quad (10)$$

is the friction velocity, z is the wind wheel height and z_0 is the roughness length parameter which depends on the landscape type as shown in Table 1.

2.3. Drive train modeling

The drive train of a WTGS comprises the wind wheel, the turbine shaft, the gearbox, and the generator's rotor shaft. The gearbox usually has a multiplication ratio between 50 and 150.

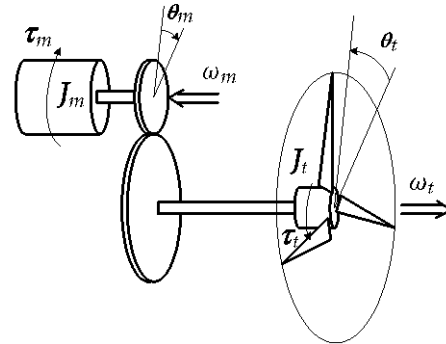


Fig.4. Two-mass drive train model.

Table 1. Values of the z_0 for different types of landscapes

Landscape type	Range of z_0 (m)
Open sea or sand	0.0001 - 0.001
Snow surface	0.001 - 0.005
Mown grass or steppe	0.001 - 0.01
Long grass or rocky ground	0.04 - 0.1
Forest, cities and hilly areas	1 - 5

Because of the high torque applied to the turbine shaft, its deformation must not be neglected and its elastic behavior should be taken into account because of its filtering properties. A common way to model the drive-train is to treat it as a series of masses connected through an elastic coupling with a linear stiffness, a damping ratio and a multiplication ratio between them. On this paper a model with two masses, graphically presented in Fig. 4, is used treating the wind wheel as one inertia J_t and the gearbox and the generator's rotor as another inertia J_m connected through the elastic turbine shaft with a k_s angular stiffness coefficient and a k_d angular damping coefficient.

$$\begin{bmatrix} \dot{\omega}_m \\ \dot{\omega}_t \\ \omega_m \\ \omega_t \end{bmatrix} = \begin{bmatrix} -k^2 k_d & k k_d & -k^2 k_s & k k_s \\ J_m & J_m & J_m & J_m \\ k k_d & -k_d & k k_s & -k_s \\ J_t & J_t & J_t & J_t \\ 1 & 0 & 0 & 0 \\ 0 & 1 & 0 & 0 \end{bmatrix} \begin{bmatrix} \omega_m \\ \omega_t \\ \theta_m \\ \theta_t \end{bmatrix} + \begin{bmatrix} 1 \\ J_m \\ 0 \\ 0 \\ 0 \\ 0 \end{bmatrix} \begin{bmatrix} \tau_m \\ \tau_t \end{bmatrix} \quad (11)$$

where θ_t and θ_m are the angles of the wind wheel and the generator shaft, ω_t and ω_m are the angular speed of the wind wheel and the generator, τ_t is the torque applied to the turbine and τ_m is the generator torque.

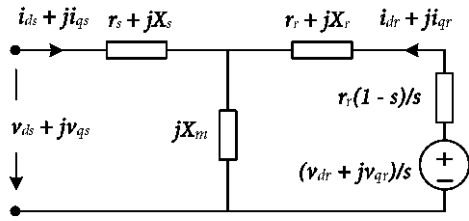


Fig.5. Equivalent circuit of a DFIG.

2.4. Generator modeling

The generator of a doubly fed WTGS is a wound rotor asynchronous machine. Assuming the stator and rotor windings to be placed sinusoidally and symmetrical, the magnetic saturation effects and the capacitance of all the windings are neglected and taking as positive the currents flowing towards the machine, the relations between the voltages on the machine windings and the currents and its first derivative may be written in a synchronous reference *qd* frame representation as:

$$\begin{bmatrix} v_{qs} \\ v_{ds} \\ v_{qr} \\ v_{dr} \end{bmatrix} = B \cdot \frac{d}{dt} \begin{bmatrix} i_{qs} \\ i_{ds} \\ i_{qr} \\ i_{dr} \end{bmatrix} + C \cdot \begin{bmatrix} i_{qs} \\ i_{ds} \\ i_{qr} \\ i_{dr} \end{bmatrix} \quad (12)$$

$$B = \begin{bmatrix} L_s & 0 & L_m & 0 \\ 0 & L_s & 0 & L_m \\ L_m & 0 & L_r & 0 \\ 0 & L_m & 0 & L_r \end{bmatrix};$$

$$C = \begin{bmatrix} r_s & \omega_s L_s & 0 & \omega_s L_m \\ -\omega_s L_s & r_s & -\omega_s L_m & 0 \\ 0 & s \omega_s L_m & r_r & s \omega_s L_r \\ -s \omega_s L_m & 0 & -s \omega_s L_r & r_r \end{bmatrix}$$

where L_s and L_r are the stator and rotor windings self-inductance coefficient, L_m is the coupling coefficient between stator and rotor windings and s is the slip.

The electromagnetic torque and the stator reactive power, which are the control objectives of the RSC control, have the following forms:

$$T_{em} = p L_m (i_{qs} i_{dr} - i_{ds} i_{qr}) \quad (13)$$

and

$$Q_s = v_{qs} i_{ds} - v_{ds} i_{qs} \quad (14)$$

where p is the number of pairs of poles of the generator. When simulating the system, expression (12) is rewritten to have the current derivatives as a function of the instantaneous currents and the applied voltages as in the usual system space-state representations.

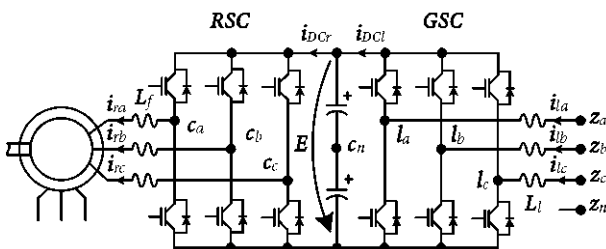


Fig.6. The rotor side and grid side converter of a DFIG.

2.5. Converter modeling

The most common topology of the converter of the DFIG is the IGBT voltage source back-to-back converter with an inverter connected to the rotor windings fed by a DC bus connected to another inverter which acts as an active rectifier connected to a three phase grid through a filter inductance in a series connection.

The dynamics of the grid side electrical circuit between the grid voltage and the voltage applied on the AC side of the converter assuming the currents positive when flowing towards the machine can be described as:

$$v_z^{abc} - v_l^{abc} = (v_{cn} - v_{zn}) \begin{bmatrix} 1 \\ 1 \\ 1 \end{bmatrix} + r_l i_l^{abc} + L_l \frac{d}{dt} i_l^{abc} \quad (15)$$

and

$$v_{cn} - v_{zn} = \frac{1}{3} (v_{za} + v_{zb} + v_{zc} - v_{la} - v_{lb} - v_{lc}) \quad (16)$$

where v_z^{abc} and v_l^{abc} are the *abc* voltage vectors of the grid and the AC side of the converter, r_l is the resistance of the filter inductors and L_l is the inductance of the filter.

The dynamics of the voltage of the DC bus can be described as:

$$E = E_0 + \frac{1}{C} \int_0^t (i_{DCI} - i_{DCr}) dt \quad (17)$$

where E is the voltage of the DC bus, i_{DCI} is the current through the DC side of the grid side inverter, i_{DCr} is the current through the DC side of the rotor side inverter and both currents can be computed by doing a power balance on each inverter.

3. CONFIGURATION AND OPERATION OF D-STATCOM

Recently, a new family of distribution STATCOM (D-STATCOM) specially adapted for distribution applications was proposed in [15], which is based on the series connection of insulate gate bipolar transistors (IGBT) and operated with pulse width modulation (PWM) techniques.

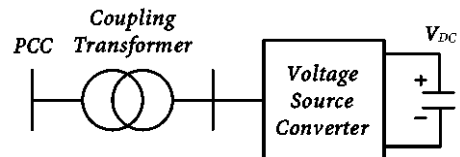


Fig.7. The structure of a D-STATCOM.

The basic principle of D-STATCOM is to use voltage source converter (VSC) technology based on power IGBT that has the capability to interrupt current flow in response to a gating command. This allows the D-

STATCOM to generate an AC voltage source at the converter terminal at the desired fundamental frequency with controllable magnitude.

The exchange of reactive power with the network is obtained by controlling the magnitude of the voltage source, whilst the exchange of active power is obtained by controlling the phase angle of the voltage source.

The active and reactive power transfer between the VSC and the grid can be expressed as follows:

$$P_{D-STATCOM} = \frac{V_1 V_2 \sin \delta}{X} \tag{18}$$

$$Q_{D-STATCOM} = \frac{V_1(V_1 - V_2 \cos \delta)}{X} \tag{19}$$

where X is the reactance of both the interconnection transformer and the D-STATCOM filter, V_1 and V_2 are voltage at PCC and D-STATCOM terminal, respectively. And δ is the angle of V_1 with respect to V_2 . The interaction between the PCC voltage and the voltage at the D-STATCOM terminals controls the reactive power flow. If the PCC voltage is less than the voltage at the D-STATCOM terminals, the D-STATCOM acts as a capacitor and reactive power is injected from the D-STATCOM to the system. On the other hand, if the PCC voltage is higher than the voltage at the D-STATCOM terminal, the D-STATCOM behaves as an inductor and the reactive power transfers from the system to the D-STATCOM. Under normal operating conditions, both voltages are equal and there is no power exchange between the D-STATCOM and the AC system.

4. CASE STUDIES

The simulation is conducted using Matlab/Simulink to further analyze the transient characteristics of DFIGs. The DFIG parameters for simulation are shown in Table 2. The parameters and the electrical variables of the DFIG are per-unit value on the stator side. The power reference of per-unit value is the rated apparent power, and the voltage reference is the rated stator phase voltage.

To analyze the effects of the transient responses on elements of studied power system, the test system is tested with two wind farms based on DFIG and conventional induction generator WTs, respectively, are integrated into existed power system under asymmetrical and symmetrical fault conditions at PCC. A fault at PCC is applied at $t = 1.5$ s and removed at $t = 1.52$ s. The rotor and the system protection are disregarded to reveal the entirety of the DFIG transient process.

The transient responses of reactive power of DFIG, IG, PCC and D-STATCOM under the symmetrical fault condition are shown in Fig. 9. It is easy to realize that the PCC reactive power always maintains stability before and during the fault due to the presence of D-STATCOM. However, after the short circuit is removed from the system at time $t = 1.52$ s, the reactive power of all the elements of the system must be subjected to strong fluctuations, and it takes long time to recover the steady state. In particular, the reactive power of the D-STATCOM at the time after the fault tends to oscillate

continuously to mitigate the negative effects to the stability of power systems caused by the transient fluctuations of reactive power of DFIG and IG.

Fig. 10 presents responses of rotor current, rotor voltage and stator voltage of DFIG under different fault conditions. To facilitate the analytical process, take an observation on the solid line under symmetrical fault. There are two different transients which can be observed:

Table 2. Parameters of DFIG and IG wind turbine

Parameters	DFIG	IG
Rated power, P_{nom} (MW)	1.5	1.5
Rated voltage, V (kV)	575	575
Rated frequency, f (Hz)	60	60
Rated slip, s	-0.2	-0.01
Pole pairs, p	3	3
Inertia constant, H_s	0.685	5.04
R_s (pu)	0.023	0.0048
X_s (pu)	0.18	0.1248
R_r (pu)	0.016	0.0044
X_r (pu)	0.16	0.1791
X_m (pu)	2.9	6.77

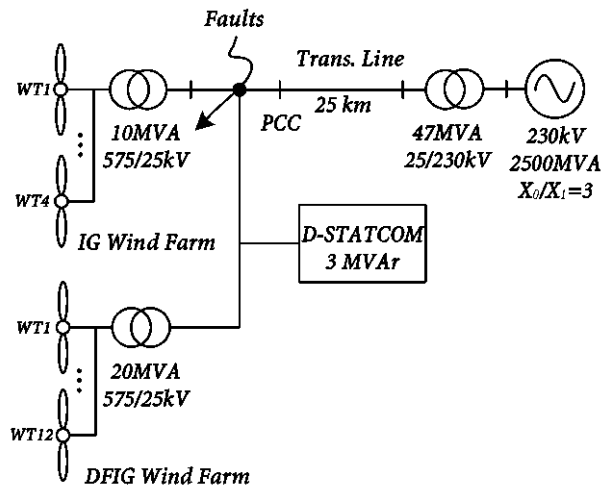


Fig. 8. Simulation power system equipped with a D-STATCOM.

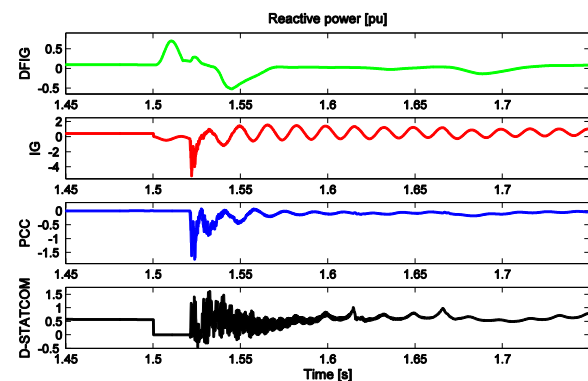


Fig.9. Reactive power of DFIG, IG, PCC and D-STATCOM under a symmetrical fault condition.

- 1) At the time $t = 1.5$ s, there was a sharp voltage drop

to zero value, followed by rotor voltage and rotor current significant oscillations. The rotor current reaches a maximum value of 5 pu while rotor voltage of DFIG also remarkably fluctuates.

2) At time after the fault clearing point, $t = 1.52$ s, the rotor and stator voltage oscillate seriously. Since the second transient had a more rapid and larger voltage drop than the first transient, hence it is more representative to explain responses of the DFIG wind turbine and the fault-clearing transient cannot be neglected.

According to Fig. 11, active power and reactive power of DFIG under symmetrical and asymmetrical fault conditions have been clearly expressed. In the case of symmetrical fault, active power value of DFIG drops to zero value, whereas in the case of asymmetrical fault, active power of DFIG only slightly fluctuates around the value of 1 pu. Similarly, reactive power of DFIG also fluctuates more sharply in the symmetrical fault case, compared to the case of the asymmetrical fault.

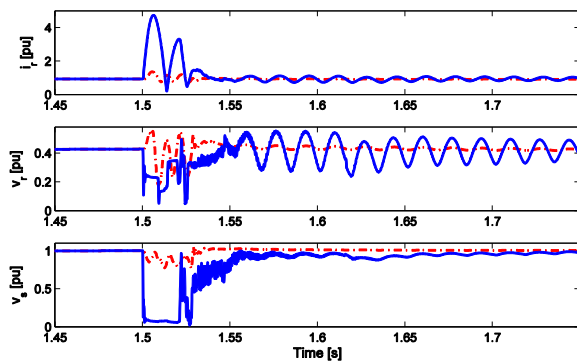


Fig.10. Response of rotor current, rotor voltage and stator voltage of DFIG under different fault conditions. Solid line: symmetrical fault and dash-dot line: asymmetrical fault.

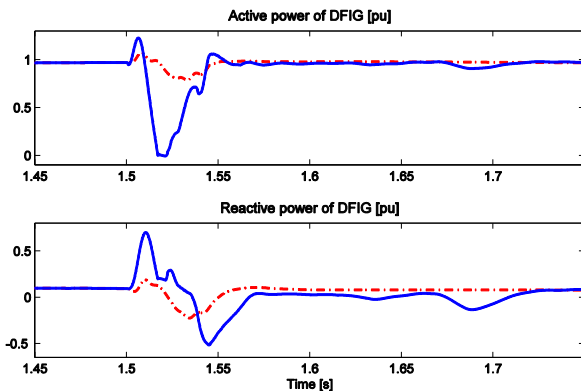


Fig.11. Active and reactive power of DFIG under different fault conditions. Solid line: symmetrical fault and dash-dot line: asymmetrical fault.

As seen in Fig. 12, at the time $t = 1.3$ s, in the symmetrical fault condition, the DC-link voltage reaches the maximum value of 1770 V. This is obviously unfavourable from a system stability point of view. On the other hand, in the asymmetrical fault condition, the maximum value of the DC-link voltage is only 1170 V. This is reason why the symmetrical fault is considered as

the most serious fault happened in the power system.

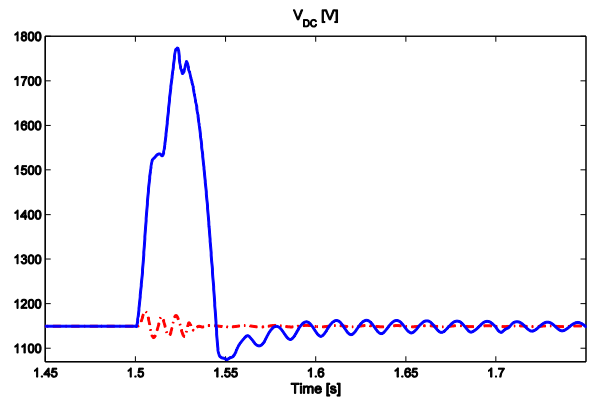


Fig.12. Response of DC voltage of DFIG under different fault conditions. Solid line: symmetrical fault and dash-dot line: asymmetrical fault.

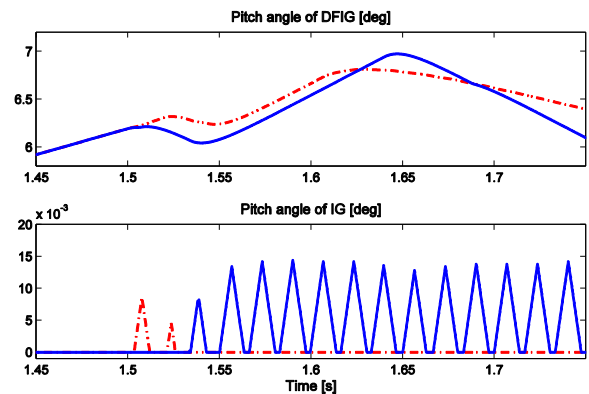


Fig.13. Pitch angle of DFIG and IG under different fault conditions. Solid line: symmetrical fault and dash-dot line: asymmetrical fault.

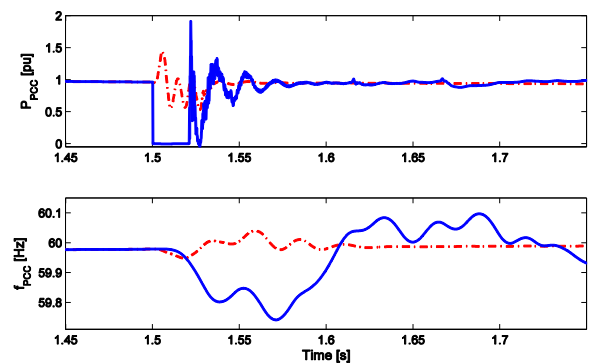


Fig.14. Transient response of active power and frequency at PCC. Solid line: symmetrical fault and dash-dot line: asymmetrical fault.

Fig. 13 shows the pitch angle responses of DFIG and IG under different fault conditions. In the symmetrical fault, the IG pitch angle controller is activated continuously to reduce the electromagnetic torque fluctuations. And after the fault is removed from the system, the pitch angle of IG still significantly oscillates before getting the zero value. Compared to the IG, the

pitch angle of DFIG changed little between the symmetrical and asymmetrical fault.

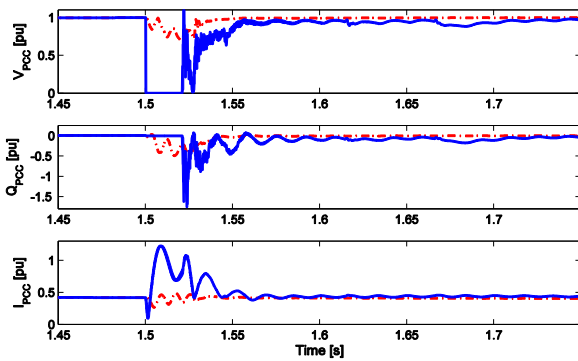


Fig. 15. Response of voltage, reactive power and current at PCC under different fault conditions. Solid line: symmetrical fault and dash-dot line: asymmetrical fault.

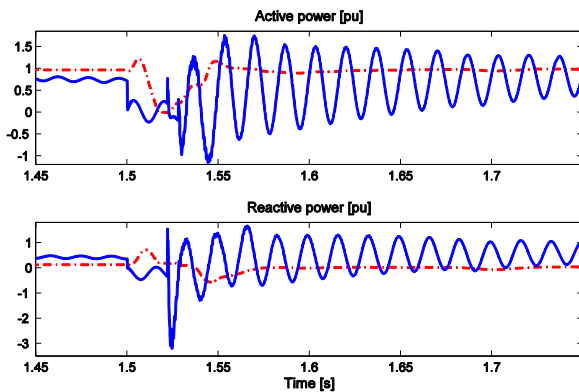


Fig.16. Active and reactive power of DFIG and IG under a symmetrical fault condition. Solid line: IG and dash-dot line: DFIG.

As shown in Fig. 14 and Fig. 15, the current oscillations affected the active power whereas the reactive power was hardly affected by the voltage oscillations. This indicates that the grid was strong enough for the voltage to be relatively insensitive to the active power oscillations. Consequently, the reactive power was influenced to a great extent by the voltage and was loosely correlated with the behavior of the active power. During an asymmetrical fault condition, the PCC voltage dropped by 30%, followed by a slow recovery and slight frequency oscillations around 60.05 Hz due to the voltage disturbances. The active power suffered oscillations of around 1.5 pu in amplitude, while the reactive power absorption decreased to -0.5 pu as a result of the voltage decay. In a symmetrical fault condition, all electrical variables at the PCC including frequency, active and reactive powers, voltage and current must face the critical oscillations, compared to the asymmetrical fault. An observation from Fig. 14 and Fig. 15 shows that the PCC voltage drops to zero value during fault time, DFIG cannot generate the active power and absorb a maximum reactive power value about 2 pu at fault clearing time. Moreover, the fluctuations of active power lead to remarkable frequency oscillations of the system.

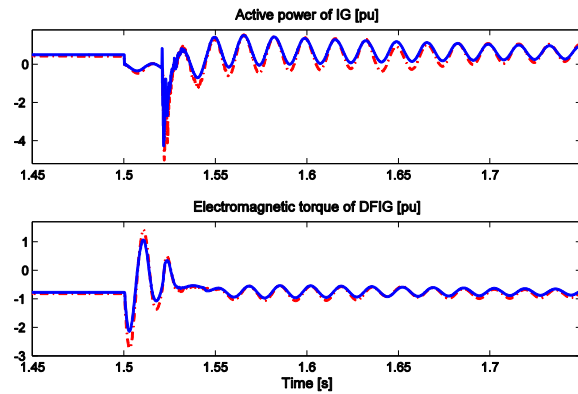


Fig.17. Comparative illustration of DFIG's Electromagnetic torque and IG's reactive power under symmetrical fault. Solid line: with D-STATCOM and dash-dot line: without D-STATCOM.

An analytical comparison of the dynamic responses of active and reactive power between DFIG and IG wind turbine under the symmetrical fault was clearly described in Fig. 16. According to Fig. 16, at the pre-fault time, the IG wind turbine was running at lower power output, which was around 0.75 pu. The IG generated reactive power of 0.5 pu. Otherwise, DFIG operated stably with active power of 1 pu and nearly do not generate reactive power.

Fig. 17 described the transient responses of the reactive power of IG and the electromagnetic torque of DFIG in with and without D-STATCOM cases under symmetrical fault. As seen in Fig. 17, the reactive power of IG and the electromagnetic torque of DFIG improved the transient oscillations due to D-STATCOM appearance. The amplitude of the reactive power of IG and the electromagnetic torque of DFIG fluctuations in with D-STATCOM case decreased remarkably compared to the without D-STATCOM case.

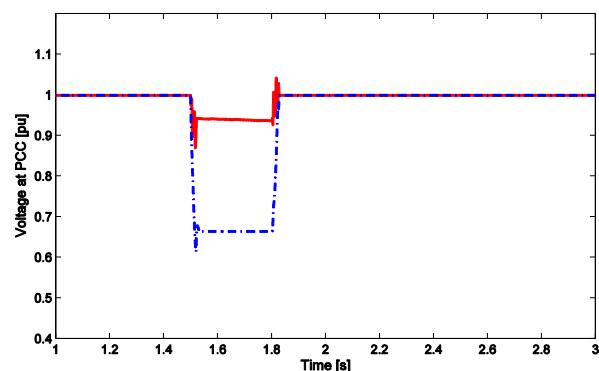


Fig.18. Illustration of the effectiveness of the D-STATCOM under asymmetrical fault. Solid line: with D-STATCOM and dash-dot line: without D-STATCOM

The illustration of the effectiveness of using the D-STATCOM to enhance the voltage profile is showed in Fig. 18. The solid line in Fig. 18 shows the response of voltage at PCC in with D-STATCOM case. In this case, the minimum voltage drops to 0.65 pu. And the dash-dot line represents the PCC voltage without the D-STATCOM. When the voltage disturbance is

compensated, the PCC voltage drops to 0.9 pu. It is so clear that D-STATCOM can be used as an effective device to improve the voltage profile under grid fault conditions.

5. CONCLUSIONS

Higher installation capacity of the DFIG wind farm brings about the wider influence of wind power on the grid and causes a major change in the operating conditions of the power systems during transient events. Transient stability is largely dominated by generator technologies in the power system, and dynamic characteristics of DFIG wind turbines are different from that of the synchronous generators in the conventional power plants. Therefore, the analysis of transient stability of power systems integrated with the DFIGs has become a very important issue.

The paper has presented a model for a WTGS based on a DFIG. A detailed modeling of wind speed, the mechanical dynamics, the WT electrical system and the converter has been presented. FRT capability of a DFIG wind turbine was also demonstrated and evaluated. In this paper, an analytical comparison of transient behaviors between DFIG and conventional induction generator WT was also presented. The comparison showed that the DFIG wind turbine had more improved FRT performance, compared to IG wind turbine under all kinds of grid faults. Besides, the effects of symmetrical and asymmetrical faults on the transient behavior of the DFIG were analyzed. The acquired transient characteristics provided good references to develop and improve DFIG control during grid faults. Based on simulation results, it can be concluded that the transient responses of DFIG and their effects on WTs' operation and behaviors of whole power system depended on kinds of fault and where the faults occur.

The application of D-STATCOM to improve the voltage profile and FRT capability of a DFIG wind generation was also investigated in this paper. The impacts of wind farm dynamics on a power system were analyzed, which showed that the integration of wind generation significantly affected the voltage stability of the system. This paper made an assessment of the effectiveness of using FACTs to improve voltage profile of DFIG wind turbine. Finally, it can be said that D-STATCOM can be used as an effective device to enhance the voltage profile of the distribution networks with distributed wind generation.

REFERENCES

- [1] M. A. Chowdhury, W. X. Shen, N. Hosseinzadeh and H. R. Pota. 2015. A review on transient stability of DFIG integrated power system. *International Journal of Sustainable Engineering*. 8 (6): 1-12.
- [2] M. Mohseni, M. A. S. Masoum, and S. M. Islam. 2011. Low and high voltage ride-through of DFIG wind turbines using hybrid current controlled converters. *Electric Power Systems Research*. 81 (7): 1456-1465.
- [3] C. Jauch, J. Matevosyan, T. Ackermann, S. Bolik. 2005. International comparison of requirements for connection of wind turbines to power systems. *Wind Energy*. 8: 295-306.
- [4] N. R. Ullah, T. Thiringer, and D. Karlsson. 2007. Voltage and transient stability support by wind farms complying with the E.ON netz grid code. *IEEE Transactions on Power Systems*. 22 (4): 1647-1656.
- [5] X. Kong, Z. Zhang, X. Yin. 2014. Study of fault current characteristics of the DFIG considering dynamic response of the RSC. *IEEE Transactions on Energy Conversion*. 29: 278-287.
- [6] J. Ouyang and X. Xiong. 2009. Dynamic behavior of the excitation circuit of a DFIG under a symmetrical voltage drop. *Renewable Energy*. 71: 629-638.
- [7] J. Hu, Y. He, L. Xu, and B. W. Williams. 2009. Improved control of DFIG systems during network unbalance using PI-R current regulators. *IEEE Transactions on Industrial Electronics*. 569 (2): 439-451.
- [8] M. S. Vicatos and J. A. Tegopoulos. 1991. Transient state analysis of a doubly-fed induction generator under three phase short circuit. *IEEE Transactions on Energy Conversion*. 6 (1): 62-68.
- [9] J. B. Ekanayake, L. Holdsworth X. G. Wu, and N. Jenkins. 2003. Dynamic modeling of DFIG wind turbines. *IEEE Transactions on Power System*. 18 (2): 803-809.
- [10] R. Koessler, S. Pillutla, L. Trinh, and D. Dickmader. 2015. Integration of large wind farms into utility grids (Part 1-Modeling of DFIG). *Proc. IEEE PES General Meeting*. 3: 1511-1519.
- [11] T. Thiringer, A. Petersson, and T. Petru. 2003. Grid disturbance response of wind turbines equipped with induction generator and doubly-fed induction generator. *Proc. IEEE PES General Meeting*. 3: 1542-1547.
- [12] M. J. Hossain, H. R. Pota, V. A. Ugrinovskii and R. A. Ramos. 2010. Simultaneous STATCOM and Pitch angle control for improved LVRT capability. *IEEE Transactions on Sustainable Energy*. 1 (3): 142-151.
- [13] N. K. Roy, M. J. Hossain and H. R. Pota. 2011. Voltage profile improvement for distributed wind generation using D-STATCOM. *IEEE PES General Meeting*. 1-6.
- [14] J. G. Slootweg. 2005. Reduced-order modelling of wind turbines. *Wind Power in Power Systems*. 555-585.
- [15] T. T. Nguyen and V. L. Nguyen. 2005. Application of wide-area network of phasor measurements for secondary voltage control in power systems with FACTs controllers. *Proc. IEEE PES General Meeting*. 3: 2927-2934.